Supporting information for:

Multi-parameter estimation in voltammetry when an electron transfer process is coupled to a chemical reaction

Alexandr N. Simonov,[‡] *Graham P. Morris,*[†] *Elena Mashkina,*[‡] *Blair Bethwaite,*[§] *Kathryn Gillow,*[†] *Ruth E. Baker,*[†] *David J. Gavaghan,*[††,*] *Alan M. Bond* [‡,*]

[‡] School of Chemistry, Monash University, Clayton, Victoria 3800, Australia

[†] Mathematical Institute, University of Oxford, Radcliffe Observatory Quarter, Woodstock Road, Oxford, OX2 6GG, UK

[§] Monash eResearch Centre, Monash University, Clayton, Victoria, 3800, Australia

[††] Department of Computer Science, University of Oxford, Wolfson Building, Parks Road, Oxford, OX1 3QD, UK

SUPPORTING INFORMATION CONTENTS

APPENDIX A. VOLTAMMETRIC SIMULATIONS METHODS AND THEORY

Simulations of d.c. and a.c. voltammograms are based on the Butler-Volmer model for electron transfer with the value of charge-transfer coefficient $\alpha = 0.50$ and the semi-infinite planar diffusion model employed to describe the mass-transport. They were undertaken using in-house software written in C code at the University of Oxford[S1,2] or the MECSim software[S3] at Monash University. Incorporation of homogeneous chemical reactions into the models was achieved in the simulations undertaken at Oxford as outlined below and in the case of the Monash work as formulated elsewhere using a generic approach based on microscopic reversibility of all reactions.[S4,S5] Extensive comparisons with simulations undertaken for the **EC** mechanism with the commercially available DigiSim (d.c. method) and DigiElch (d.c. and a.c methods) software over a wide parameter range revealed concordance in current-potential-time data to at least 4 significant figures.

Details of theory used with the 'Global Method' of data analysis

An **EC** reaction with the **E** step as oxidation proceeds according to

$$A \underset{\longleftarrow}{\overset{E^0, k^0, \alpha}{\longrightarrow}} B + e^-,$$

$$B \underset{k^b}{\overset{k^f}{\rightleftharpoons}} C, \tag{A1}$$

where k^f and k^b (units s^{-1}) represent the forward and backward rate constants of the chemical reactions, respectively.

For our three species A, B and C with concentrations given by c_A, c_B and c_C, respectively, we have the equations

$$\frac{\partial c_A}{\partial t} = D_A \frac{\partial^2 c_A}{\partial x^2}, \tag{A3}$$

$$\frac{\partial c_B}{\partial t} = D_B \frac{\partial^2 c_B}{\partial x^2} - k^f c_B + k^b c_C, \tag{A4}$$

$$\frac{\partial c_C}{\partial t} = D_C \frac{\partial^2 c_C}{\partial x^2} - k^b c_C + k^f c_B, \quad x > 0, t > 0, \tag{A5}$$

where t is time and x is distance from the electrode surface, and D_A, D_B and D_C are the diffusion coefficients of the species A, B and C, respectively. The reaction terms are derived assuming the law of mass action applies to the chemical step of Equation (A1). The initial and boundary conditions are:

$$c_A(x,0) = c_\infty, \tag{A6}$$

$$c_B(x,0) = 0, \tag{A7}$$

$$c_C(x,0) = 0 \text{ at } x \geq 0 \tag{A8}$$

$$c_A \to c_\infty \text{ as } x \to \infty, \quad t > 0, \tag{A9}$$

$$c_B \to 0 \text{ as } x \to \infty, \quad t > 0, \tag{A10}$$

$$c_C \to 0 \text{ as } x \to \infty, \quad t > 0, \tag{A11}$$

The conservation and flux conditions at the electrode surface ($x = 0$) for $t > 0$

$$FAD_A \frac{\partial c_A}{\partial x} = -FAD_B \frac{\partial c_B}{\partial x} = I_f, \tag{A12}$$

$$D_C \frac{\partial c_C}{\partial x} = 0, \tag{A13}$$

also apply along with the the Butler-Volmer condition

$$I_f = FAk^0 \left[c_A \exp\left(\frac{(1-\alpha)F}{RT}(E(t)-E^0) \right) - c_B \exp\left(\frac{-\alpha F}{RT}(E(t)-E^0) \right) \right], \tag{A14}$$

where I_f is the faradaic current.

With the assumption of equal diffusion coefficients, *viz.* $D = D_A = D_B = D_C$, we have

$c_A + c_B + c_C = c_\infty$, and we can reduce the number of variables by one. To complete the model, our

final equations are

$$E(t) = E_{\text{applied}}(t) - I_{\text{total}}(t)R_u, \tag{A15}$$

$$E_{\text{applied}}(t) = E_{\text{start}} + vt + \Delta E \sin(2\pi ft) \tag{A16}$$

$$I_{\text{total}}(t) = I_c(t) + I_f(t), \tag{A17}$$

$$I_c(t) = C_{\text{dl}} \frac{dE(t)}{dt}, \tag{A18}$$

where $E(t)$, $E_{\text{applied}}(t)$ and E_{start} are the real, applied and starting potentials at the working

electrode, I_{total} is the total current comprised of I_f and capacitive component I_c, R_u is the

uncompensated resistance, C_{dl} is the double-layer capacitance, v is the d.c. potential scan rate,

ΔE and f are the amplitude and frequency of the a.c. perturbation.

We non-dimensionalise the equations exactly as in previous publication[S6] and also using the

relationships

$$k^{f*} = \frac{RT}{Fv} k^f, \tag{A19}$$

$$k^{b*} = \frac{RT}{Fv} k^b. \tag{A20}$$

In terms of non-dimensional variables, with u and w representing the non-dimensional

concentrations of A and B, respectively, we now have

$$\frac{\partial u}{\partial t} = \frac{\partial^2 u}{\partial x^2}, \tag{A21}$$

$$\frac{\partial w}{\partial t} = \frac{\partial^2 w}{\partial x^2} - k^{f*}w + k^{b*}(1-u-w), \quad x>0, t>0. \tag{A22}$$

Note here that time t and space x are also now non-dimensional variables as defined in Eq. 5 of reference S6, but we avoid a change of notation for clarity and simplicity. In non-dimensional variables, the initial and boundary conditions become

$$u(x,0) = 1, \tag{A23}$$

$$w(x,0) = 0, \quad x \geq 0, \tag{A24}$$

$$u \rightarrow 1, \tag{A25}$$

$$w \rightarrow 0, \quad \text{as} \quad x \rightarrow \infty, t > 0, \tag{A26}$$

and for $x = 0$, $t > 0$

$$\frac{\partial u}{\partial x} = -\frac{\partial w}{\partial x} = I_{\text{f}}, \tag{A27}$$

$$I_{\text{f}} = k^0 \left[u \exp\left((1-\alpha)(E(t)-E^0)\right) - w \exp\left(-\alpha(E(t)-E^0)\right) \right] \tag{A28}$$

Non-dimensionalised versions of Equations (A15) to A(18) complete the model in as described in reference S6.

This system of one-dimensional partial differential equaitions is solved using the finite difference method, as described in earlier work.[S6,7] In the current case, the Butler-Volmer equation contains both u and w so we must find expressions for both of these variables in terms of I_{total}, and then substitute back into Equation (A28). Using the same notation as in our earlier work, with U_j^m and W_j^m representing the finite difference numerical approximation to $u(x = j\Delta x, t = m\Delta t)$ and $w(x = j\Delta x, t = m\Delta t)$, respectively, and $\mu = \Delta t/(\Delta x)^2$, we discretise both Equations (A23) and (A24), and use an explicit approximation for the source and sink terms, to give for $1 \leq j \leq N-1$ and $m \geq 0$:

$$-\theta\mu U_{j-1}^{m+1} + (1+2\theta\mu)U_j^{m+1} - \theta\mu U_{j+1}^{m+1} = (1-\theta)\mu U_{j-1}^m + (1-2(1-\theta)\mu)U_j^m + (1-\theta)\mu U_{j+1}^m \tag{A29}$$

and

$$-\theta\mu W_{j-1}^{m+1} + (1+2\theta\mu)W_j^{m+1} - \theta\mu W_{j+1}^{m+1} =$$

$$= (1-\theta)\mu W_{j-1}^m + (1-2(1-\theta)\mu)W_j^m + (1-\theta)\mu W_{j+1}^m - k_f dt W_j^m + k_b dt U_j^m, \tag{A30}$$

where $\theta = 0.5$.

In practice, this approximation is acceptable (in the sense that numerical errors are very much smaller than experimental error) provided a sufficiently small time step is used. We have checked that for all simulations described in this paper; the numerical solution no longer varies with a further reduction in the time or space step. In addition, the approximation simplifies the solution as the equations are then decoupled. From here on, the Thomas algorithm[S8] applies to both Equations (A29) and (A30), leading to equations of the form

$$U_0^{m+1} = h_U(I_f^{m+1}), \tag{A31}$$

$$W_0^{m+1} = h_V(I_f^{m+1}), \tag{A32}$$

for known functions h_U and h_W, which can be substituted into the discretised version of Equation (A28), and rearranged to give

$$g(I_{total}^{m+1}) = 0, \tag{A33}$$

for a known function g. Brent's method[S9] can then be applied to solve for the total current, I_{total}^{m+1}, at each subsequent time-step.
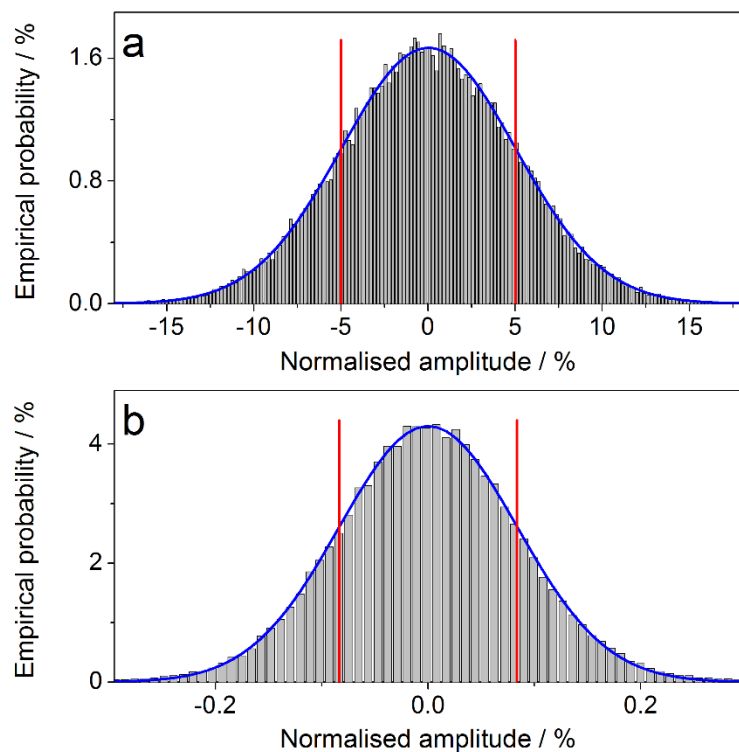
Figure S1. Magnitude distribution of noise (a) added to simulated a.c. voltammograms relevant to Tables 1-3, Figs. 1, S2 and S3 and Appendix B and (b) recovered from the experimental a.c. voltammogram obtained for reduction of *trans*-stilbene at $f = 9$ Hz (grey bars). Blue curves are the best fit normal distribution to the experimental data; red lines show 1 standard deviation interval with respect to the mean value. Noise amplitude is normalised to the peak total current in the a.c. voltammogram.

APPENDIX B. RATIONALE FOR CHOICE OF PARAMETERS USED IN ANALYSIS OF

THE SIMULATED DATA WITH 5% ADDED NOISE

Using the mathematical models and numerical solution schemes described in the main text, potentially difficult parameter recovery regimes applicable in d.c. voltammetry with the **EC** mechanism were identified. Simulated data used in this exercise had a scan rate of 0.100 V s^{-1} and a diffusion coefficient of $2 \cdot 10^{-5}$ cm^2 s^{-1}, which represent values that commonly apply in experimental studies. Five different regimes of k^0 were selected corresponding to fully reversible ($k^0 = 10^3$ cm s^{-1}), quasi-reversible ($k^0 = 10^{-1}$, 10^{-2} and 10^{-4} cm s^{-1}) and irreversible ($k^0 = 10^{-6}$ cm s^{-1}) electron transfer kinetics. At each regime, four values of k^f (0.1, 1, 10 and 100 s^{-1}) and five values of k^b (0, 0.1, 1, 10 and 100 s^{-1}) were used, with $k^b = 0$ s^{-1} representing an irreversible chemical reaction step. In the cases of an irreversible chemical reaction and at the chosen scan rate, these values of k^f correspond to $\lambda = 0.026$ ($k^f = 0.1$ s^{-1}), $\lambda = 0.26$ ($k^f = 1$ s^{-1}), $\lambda = 2.6$ ($k^f = 10$ s^{-1}) and $\lambda = 26$ ($k^f = 100$ s^{-1}), and so they encompass the region in which sensible parameter estimation should be possible if the electron transfer step is reversible, according to Saveant.[S10]

For each combination of parameters, the backwards to forwards peak current ratio, the potentials at which they occur, the mid-point potential (average of oxidation and reduction peak potentials and the peak-to-peak separation (difference in oxidation and reduction peak potentials) were recorded. In addition, at each value of k^0, reference measurements for an **E** reaction, *i.e.* electron transfer with no coupled chemical reaction, were used for comparison. In further discussion within the given appendix, the **EC** mechanism described by equation 2 (main text) with **E** as an oxidation process is considered.

The switching potentials of simulations were varied for the different regimes of k^0. For the oxidation case considered, the switching potential, E_{switch}, was chosen to be approximately 0.5 V greater than the oxidation peak potential of the **E** reaction at that value of k^0, and the starting and final potentials, E_{start} and E_{final}, respectively, were chosen such that the companion reduction peak would be visible.

In simulations of d.c. cyclic voltammograms with $k^0 = 10^3$ cm s^{-1} and $k^0 = 10^{-1}$ cm s^{-1} (indistinguishable from and close to the reversible limit under chosen conditions, respectively) and $k^f > 0$ s^{-1} and $k^b = 0$ s^{-1}, as k^f is increased, the peak current magnitude ratio decreases as the reduction peak current heads to zero, and the position of the oxidation peak becomes more negative, particularly at higher values of k^f, as seen in Fig. B1.
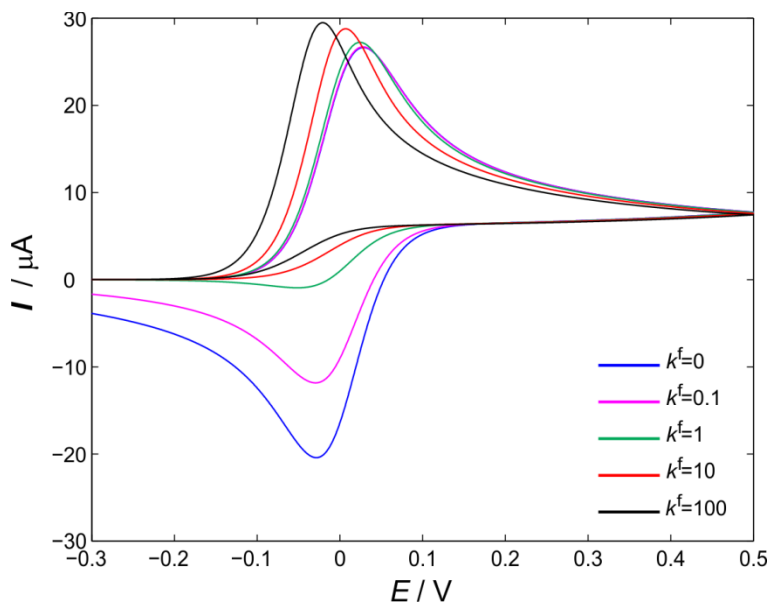

Figure B1. The effect of increasing k^f in simulations of d.c. cyclic voltammetry, with $k^0 = 10^3$ cm s^{-1} and $k^b = 0$ s^{-1}. Other parameters as defined in Table 1 (main text).

When $k^f \geq k^b > 0$ s^{-1}, the d.c. voltammetric characteristics vary with both the ratio $K = k^f/k^b$, where K is the equilibrium constant, and the sum $L = k^f + k^b$. With K constant, increasing L results in a larger ratio and more negative peak potentials, while for a fixed value of k^b,

increasing k^f (and hence K) results in a similar behaviour to the $k^b = 0$ s^{-1} case, where the peak current ratio approaches a limiting value corresponding to the disappearance of the reduction peak, as well as the oxidation peak occurring at a more negative potential.

With $k^0 = 10^{-2}$ cm s^{-1}, corresponding to a clearly quasi-reversible electron transfer reaction, and with $k^b = 0$ s^{-1}, again increasing k^f rapidly causes the reduction peak to disappear, but in this case, further increases also result in a lessening in magnitude of the oxidation peak current, as shown in Figure B2. In the case of this **EC$_{irrev}$** reaction, increases in k^f also shift the oxidation peak to more negative potentials.
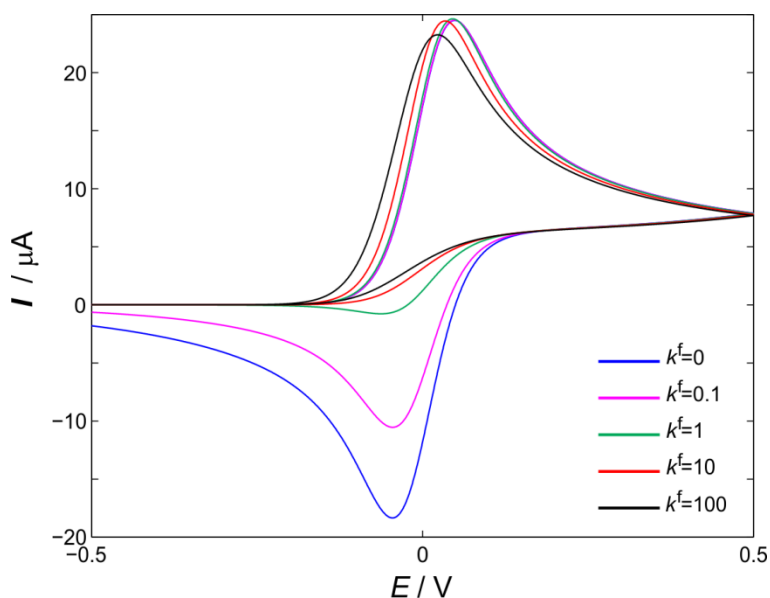

Figure B2. The effect of increasing k^f in simulations of d.c. cyclic voltammograms with $k^0 = 10^{-2}$ cm s^{-1} and $k^b = 0$ s^{-1}. Other parameters are as defined in Table 1 (main text).

With $k^0 = 10^{-4}$, the immediately obvious pattern detected in d.c. cyclic voltammograms is that there is no variation at all in the oxidation peak position with k^f when $k^b = 0$, nor indeed the current peak magnitude or peak shape as shown in Figure B3. However, changes in the chemical reaction rate parameters k^f and k^b still result in changes to the reduction peak current and position with trends such as the reduction peak disappearing when $k^f \geq k^b$ again being apparent.
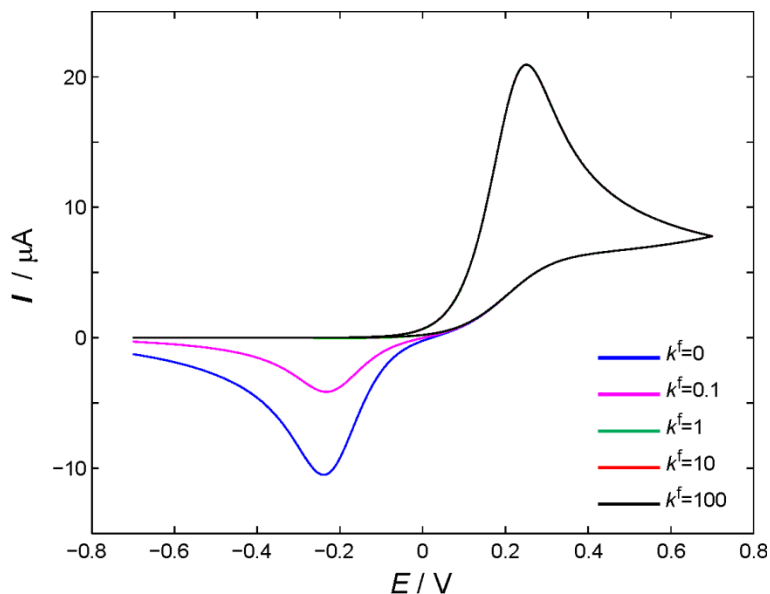
Figure B3. The effect of increasing k^f in simulations of d.c. cyclic voltammograms with $k^0 = 10^{-4}$ cm s^{-1} and $k^b = 0$ s^{-1}. Other parameters are as defined in Table 1 (main text).

In the case of an extremely irreversible electron transfer step such as happens with $k^0 = 10^{-6}$ cm s^{-1}, with no reduction peak detected, not only are k^f and k^b unidentifiable using d.c. voltammetry, any suitable combination of these parameters in a simulation model would fit the experimental data, with the **E** and **EC** mechanisms being indistinguishable.[S11] On the basis of the above findings, the choice was made to analyse 'noisy' simulated data in the stiff but probably not totally intractable regimes with $k^0 = 10^3$ (reversible case) or 10^{-2} cm^2 s^{-1} (quasi-reversible case) and with k^f and k^b in the range of 0 to 100 s^{-1}.

A few examples of a.c voltmamograms obtained under conditions that were identified as difficult by the d.c. method were selected and the ability to accurately estimate the system parameters using the GM was examined with respect to both the d.c. and a.c. methods. In order to make the exercise not only non-trivial, but also to have it bear more resemblance to an actual experiment, simulated experimental data using the selected parameters were now perturbed by

adding noise at a level of 5% of the peak current. The equivalent exercise with the Nimrod/O tool kit leads to analogous conclusions but not quantitively identical results (see main text).

The first example considered with noisy data corresponds to a fully reversible electron-transfer reaction (simulated with $k^0 = 10^3$ cm s^{-1} and $\alpha = 0.50$) followed by a reversible chemical reaction with $k^f = k^b = 100$ s^{-1}. This is the $E_{fr}C_{rev}$ case identified in the analysis of d.c. voltammetry presented above with characteristics that lie very close to those predicted for an almost reversible E_{rev} reaction with no coupled chemical step, but with a different value of E^0.

Separate exercises with this noisy simulated data were undertaken using either d.c. or a.c. voltammetry ($f = 9$ Hz), and attempts were made to fit up to four different models: E_{fr} (parameter optimised was E^0 with k^0 and α fixed at 10^3 cm s^{-1} and 0.50, respectively), E_{qr} (parameters optimised were E^0, k^0 and α), $E_{fr}C_{rev}$ (parameters optimised were E^0, k^f and k^b, with k^0 and α fixed at 10^3 cm s^{-1} and 0.50, respectively) $E_{qr}C_{rev}$ (parameters optimised were E^0, k^0, α, k^f and k^b). The results of some of these parameter fitting exercises are included in the main text in Table 1, and also for convenience here in Table B1. The d.c. cyclic voltammetric technique in this example is unable to distinguish between the incorrect E_{fr} and $E_{qr}C_{rev}$ or correct $E_{fr}C_{rev}$ mechanisms on the basis of magnitudes of Ψ_{GM} values nor to to correctly identify the parameters even when the correct $E_{fr}C_{rev}$ model is used. In contrast, with use of the a.c technique all parameters can be found with a reasonable degree of accuracy when fitting with the $E_{fr}C_{rev}$ model. Thus, an E^0 value of 0.000V is recovered precisely, and the discrepancies in expected values of 100 s^{-1} *versus* k^f and k^b recovered ones of 115 and 111 repectively (Table B1) are not large. As expected, when fitting data simulated with the $E_{fr}C_{rev}$ model, use of the $E_{qr}C_{rev}$ model recovers values of k^0 and α that are 'incorrect' but the apparentt k^0 value of 2.0 s^{-1} still lies within

the 'fully reversible' regime, and assignment as an **E**$_{\mathbf{fr}}$**C**$_{\mathbf{rev}}$ process is the most appropriate

anyway.

Table B1. Parameters recovered from the GM-assisted fitting of designated models to the a.c.

voltammetric data simulated using an **E**$_{\mathbf{fr}}$**C**$_{\mathbf{rev}}$ reaction mechanism (equation 2; **E** as an oxidation

process) with $E^0 = 0.000$ V, $k^0 = 10^3$ cm s^{-1}, , $\alpha = 0.5$, $k^f = 100$ s^{-1} and $k^b = 100$ s^{-1} for d.c. and a.c.

voltammetry.[a]

Model	E^0 / V	k^0 / cm s^{-1}	α	k^f / s^{-1}	k^b / s^{-1}	$10^7 \cdot \Psi_{GM}$
E$_{\mathbf{fr}}$	-0.011	n.a.[b]	n.a.	n.a.	n.a.	8.8
E$_{\mathbf{qr}}$	-0.017	0.065	0.00	n.a.	n.a.	4.2
E$_{\mathbf{fr}}$**C**$_{\mathbf{rev}}$	0.000	n.a.	n.a.	115	111	4.2
E$_{\mathbf{qr}}$**C**$_{\mathbf{rev}}$	0.000	2.0	0.61	98	99	4.2

[a] Other parameters used in the simulation were $E_{start} = E_{final} = -0.3$ V, $E_{switch} = 0.5$ V, $v = 0.1$ V s^{-1}, $A = 0.07$ cm^2, $c_A = 1$ mM, $c_B = c_B = 0$ mM, $D_A = D_B = D_C = 2 \cdot 10^{-5}$ cm^2 s^{-1}, $T = 296$ K, $R_u = 0$ Ω, $C_{dl} = 0$ μF cm^{-2}, $\Delta E = 0.080$ V and $f = 9$ Hz. [b]n.a.= not applicable

It is noted that when fitting the "noisy" simulated **E**$_{\mathbf{fr}}$**C**$_{\mathbf{rev}}$ data with the **E**$_{\mathbf{qr}}$, **E**$_{\mathbf{fr}}$**C**$_{\mathbf{rev}}$ and **E**$_{\mathbf{qr}}$**C**$_{\mathbf{rev}}$

mechanisms, that the GM objective functions are of similar magnitude (Table B1). The lack of

ability to distinguish between these **E** and **EC** models on the basis of Ψ_{GM} using the automated

time-domain parameter estimation method is due to different models being able to compensate

for the added noise in different ways and end up with a close to equally good fit. This inability to

correctly determine model parameters and, as a result, the inability to identify the most

appropriate model to fit the data, is an example of practical unidentifiability. Nevertheless, when

simulations are performed based on each model using recovered parameter values reported in

Table B1 and the resolved higher order harmonics are examined visually, it is clear that

significant differences exist between the predictions from the different models when assessed

from this perspective. In the example given in Figure B4, the fifth harmonic simulated using parameters deduced on the basis of GM data optimisation using the $\mathbf{E_{qr}}$ model is clearly seen to be different to that derived from the $\mathbf{E_{qr}C_{rev}}$ one and both would be rejected heuristically in favour of the $\mathbf{E_{fr}C_{rev}}$ model if a visual check were performed versus the fifth harmonic 'expermental' data with 5% added noise, even though all three produce the same Ψ_{GM} value of $4.2 \cdot 10^{-7}$ at the 2 significant figure level (Table B1) with data analysis undertaken on the total a.c. current.
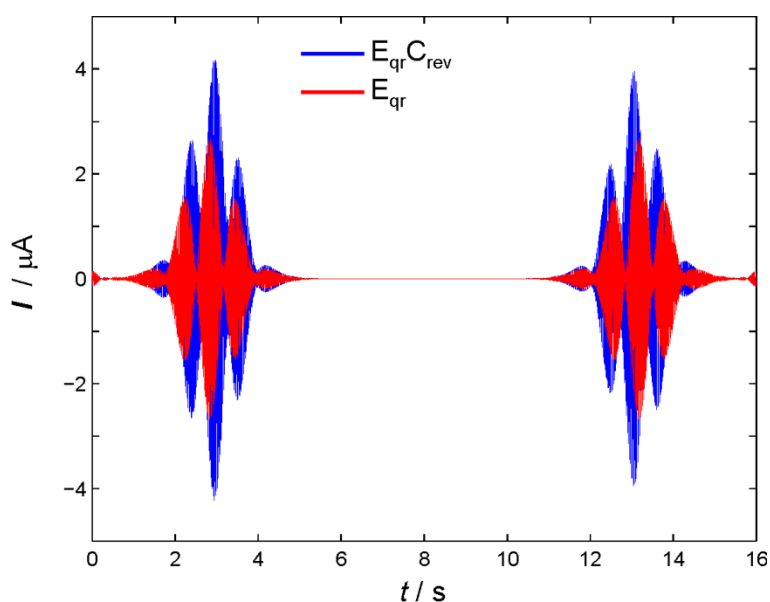

Figure B4. The 5th harmonic components of simulated a.c. voltammograms using parameters taken from the $\mathbf{E_{qr}}$ (*red*) and $\mathbf{E_{qr}C_{rev}}$ (*blue*) models in Table B1 show a clear difference even though Ψ_{GM} values are indistinguishable at the 2 significant figure level

In a second example, quasi-reversible electron transfer with $k^0 = 10^{-2}$ cm s^{-1}, followed by reasonably slow reversible chemical reactions with $k^f = 10$ s^{-1} and $k^b = 1$ s^{-1} is considered with 5% noise. In the d.c. case, with no noise, the ratio of oxidation and reduction peak currents of simulated data lie in what can be regarded as the easily 'identifiable' regime, but where in presence of 5% noise errors may emerge. The results that are included in Table 2 of the main

text, as well as in Table B2 for convenience, reveal that in this regime with 5% added noise, both the a.c. and d.c. techniques recover parameters with reasonable accuracy, with a.c voltammetry remaining slightly superior. It is also worth noting in this context that the 'small' error in the estimation of E^0 in d.c. voltammetry almost by definition has a follow-on effect on the estimates of the other parameters, as k^0 is defined to be the value at E^0.

Table B2. Parameters recovered from the GM-assisted fitting of the $\mathbf{E_{qr}C_{rev}}$ model to data simulated using an $\mathbf{E_{qr}C_{rev}}$ reaction mechanism (equation 2; $\mathbf{E}$ as an oxidation process) with $E^0 = 0.000$ V; $\alpha = 0.50$, $k^0 = 1.0 \cdot 10^{-2}$ cm s^{-1}, $k^f = 10$ s^{-1} and $k^b = 1.0$ s^{-1} for d.c. and a.c. voltammetry.[a]

Mode	E^0 / V	$10^2 \cdot k^0$ / cm s^{-1}	α	k^f / s^{-1}	k^b / s^{-1}	$10^7 \cdot \Psi$
d.c.	-0.004	0.89	0.49	6.97	0.83	0.12
a.c.	0.000	0.99	0.50	9.91	0.99	1.0

[a] Other parameters used in the simulation are $E_{start} = -0.500$ V, $E_{max} = 0.500$ V, $v = 0.100$ V s^{-1}, $A = 0.07$ cm^2, $c_A = 1.0$ mM, $c_B = c_B = 0$ mM, $D_A = D_B = D_C = 2 \cdot 10^{-5}$ cm^2 s^{-1}, $T = 296$ K, $R_u = 0$ Ω and $C_{dl} = 0$ µF cm^{-2} and for the a.c voltammetry, $\Delta E = 0.080$ V and $f = 9$ Hz.

The final example is related to that considered above. However, now the quasi-reversible electron transfer with $k^0 = 10^{-2}$ cm s^{-1} is followed by an irreversible chemical reaction with $k^f = 10$ s^{-1} ($k^b = 0$ instead of 1 s^{-1}). Again, both d.c. and a.c. voltammetric simulations have been run with 5% noise, but on this occasion each have been fitted to $\mathbf{E_{qr}C_{rev}}$ and $\mathbf{E_{qr}C_{irrev}}$ models. The results of doing this are included in Table B3 and also in Table 3 of the main text. The first observation to make in this exercise is that no significant differences exist in the a.c. or d.c. data optimisation outcome whether an attempt is made to fit the noisy simulated data with a reversible or irreversible chemical reaction step. However, when the $\mathbf{E_{qr}C_{rev}}$ model is used, the reported values of k^b are such that the ratio $K = k^f = k^b$ appears to be about 1000, which correctly implies that the backwards reaction is of negligible importance. Thus, while genereally similar levels of

accuracy in parameter recoveries are obtained from both d.c. and a.c. voltammetric simulations, the key parameter E^0 is again slightly more accurately estimated *via* a.c. voltammetry.

Table B3. Parameters recovered from the GM-assisted fitting different models to data simulated using an $\mathbf{E_{qr}C_{irrev}}$ reaction mechanism (equation 2; **E** as an oxidation process) with $E^0 = 0.000$ V; $\alpha = 0.50$, $k^0 = 1.0 \cdot 10^{-2}$ cm s^{-1}, $k^f = 10$ s^{-1} and $k^b = 0$ s^{-1} for d.c. and a.c. voltammetry.[a]

Mode	Model	E^0 / V	$10^2 \cdot k^0$ / cm s^{-1}	α	k^f / s^{-1}	k^b / s^{-1}	$10^7 \cdot \Psi$
d.c.	$\mathbf{E_{qr}C_{rev}}$	0.003	0.94	0.49	8.2	0.0024	0.12
	$\mathbf{E_{qr}C_{irrev}}$	-0.002	0.92	0.49	9.6	n.a.	0.12
a.c.	$\mathbf{E_{qr}C_{rev}}$	0.001	1.0	0.50	11	0.0011	0.99
	$\mathbf{E_{qr}C_{irrev}}$	-0.001	0.99	0.50	9.4	n.a.	0.99

[a] Other parameters used in the simulation are $E_{start} = -0.500$ V, $E_{max} = 0.500$ V, $v = 0.100$ V s^{-1}, $A = 0.07$ cm^2, $c_A = 1.0$ mM, $c_B = c_B = 0$ mM, $D_A = D_B = D_C = 2 \cdot 10^{-5}$ cm^2 s^{-1}, $T = 296$ K, $R_u = 0$ Ω and $C_{dl} = 0$ µF cm^{-2} and for the a.c voltammetry, $\Delta E = 0.080$ V and $f = 9$ Hz.

Material presented above related to a.c. voltammetric parameter recovery is derived from GM optimisation applied to the total current time-domain data format. The alternative method used in the main text for analysis of a.c voltammetric data requires transformation of the time domain response to the frequency domain and then resolving into a.c. harmonics prior to undertaking data optimisation with the Nimrod/O tool kit. Harmonic resolution is achieved by a Fourier transform - band selection and filterring - inverse Fourier transform series of operations. Results of parameter recovery using the frequency domain concept (filtered data) with the Nimrod/O tool on simulated data with 5% noise are compared with the time domain (GM) approach in the main text. Differences found in validity of parameter recovery are marginal, but brief acknowledgement of the insights available in the frequency domain approach are displayed above in Figure B4 and also in Figure B5, which shows the impact of changes in k^f on the 2nd and 5th harmonics, respectively, for an $\mathbf{E_{qr}C_{irrev}}$. In the range displayed, there is an obvious

visually detectable effect of variation in k^f. The various peaks in the harmonics become smaller compared with the case of no coupled chemical reaction (represented in blue as $k^f = 0$ s^{-1}), and the rate of decline in magnitude is harmonic-dependent. Observations of this nature confirm that a heuristic approach to parameter estimation, performed by an experienced operator, can still be implemented, and even used as a guide or reference against which to test the results of automated parameter recovery algorithms.
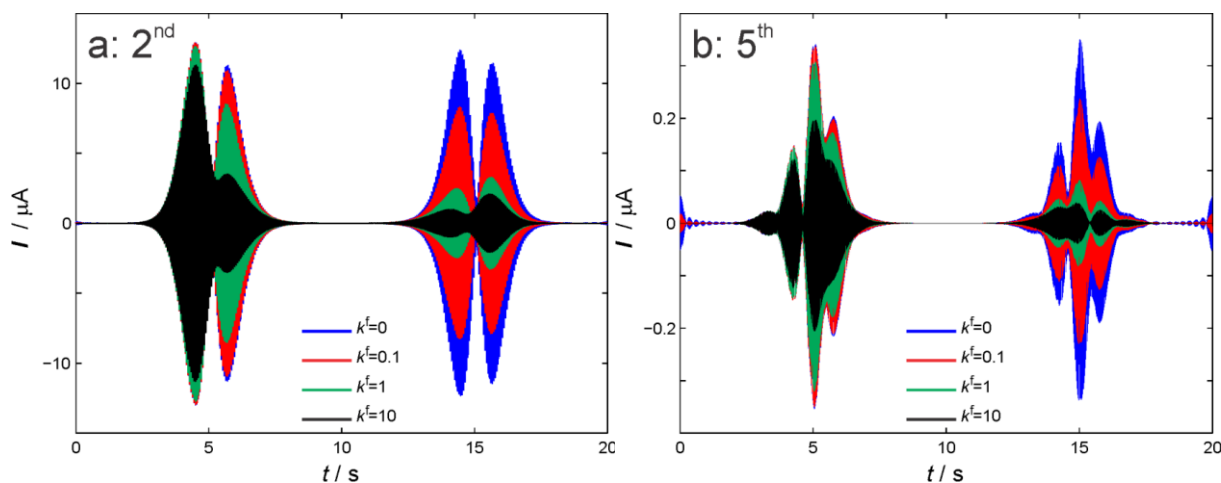

Figure B5. The effect of k^f on (a) 2nd and (b) 5th harmonic components of an a.c. voltammogram for an $\mathbf{E_{qr}C_{irrev}}$ reaction mechanism (equation 2; $\mathbf{E}$ as an oxidation process). Other parameters used in the simulations are: $E_{start} = E_{final} = -0.500$ V, $E_{switch} = 0.500$ V, $E^0 = 0.000$ V, $k^0 = 1.0 \cdot 10^{-2}$ cm s^{-1}, $\alpha = 0.50$, $v = 0.100$ V s^{-1}, $\Delta E = 0.080$ V, $f = 9.0$ Hz, $A = 0.07$ cm^2, $c_A = 1.0$ mM, $c_B = c_C = 0$ mM, $D_A = D_B = D_C = 2 \cdot 10^{-5}$ cm^2 s^{-1}, $T = 296$ K, $R_u = 0$ Ω and $C_{dl} = 0$ μF cm^{-2}.

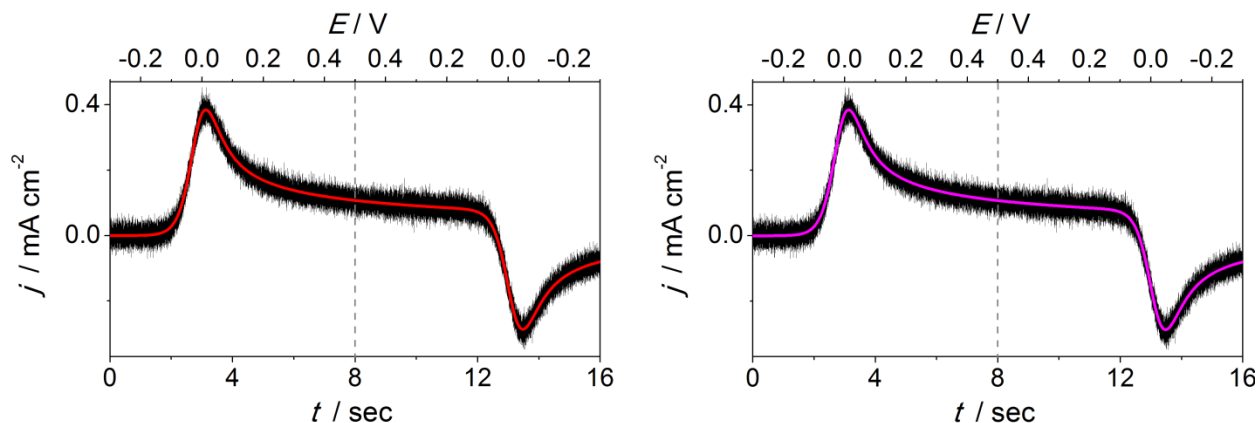**Figure S2.** A d.c. cyclic voltammogram ($v = 0.100$ V s^{-1}) simulated for an $\mathbf{E_{fr}C_{rev}}$ mechanism (equation 2, **E** as oxidation; $k^0 = 10^3$ cm s^{-1}, $k^f = k^b = 100$ s^{-1}) without (*red*) and with added noise (5% of the peak current) (*black*) and d.c. cyclic voltammogram simulated using the parameters derived by fitting the $\mathbf{E_{qr}C_{rev}}$ model to the *black* data using a particular run of Nimrod/O that achieve $\Psi_{Nim} = 0.12$ ($E^0 = 0.0105$ V, $\alpha = 0.60$, $k^0 = 8.9 \cdot 10^3$ cm s^{-1}, $k^f = 581$ s^{-1} and $k^b = 288$ s^{-1}) (*magenta*). Other simulation parameters are specified in Table 1. Currents are normalised to the electrode surface area. Dashed lines (----) indicate the time at which the direction of the d.c. potential ramp is reversed.

Figure S3. (a) Total current, (b) aperiodic component, (c) 2nd and (d) 5th a.c. harmonic components of an a.c. cyclic voltammogram (f = 9.00 Hz; ΔE = 0.080 V; v = 0.100 V s^{-1}) simulated for an $\mathbf{E_{fr}C_{rev}}$ mechanism (equation 2, $\mathbf{E}$ as an oxidation process; k^0 = 10^3 cm s^{-1}, $k^f = k^b$ = 100 s^{-1}) with added noise (5% of the peak current) (*black*) and a.c. cyclic voltammogram simulated using the parameters derived by fitting the $\mathbf{E_{qr}C_{rev}}$ model in one particular run to the *black* data using Nimrod/O that achieves the minimum value of Ψ_{Nim} = 0.096 (E^0 = 0.0037 V, α = 0.56, k^0 = 6.5·10^3 cm s^{-1}, k^f = 190 s^{-1} and k^b = 146 s^{-1}) (*magenta*). Other simulation parameters are specified in Table 1. Currents are normalised to the electrode surface area. Dashed lines (----) indicate the time at which the direction of the d.c. potential ramp is reversed.
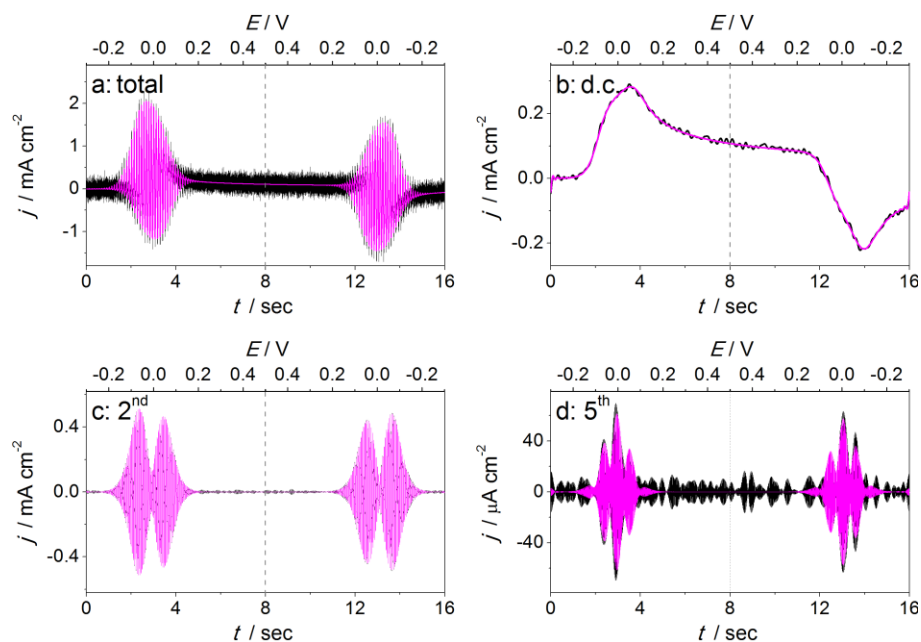
Figure S4. (a) Total current, (b) aperiodic component, (c) 2nd and (d) 5th a.c. harmonic components of an a.c. cyclic voltammogram ($f = 9.00$ Hz; $\Delta E = 0.080$ V; $v = 0.100$ V s^{-1}) simulated for an $\mathbf{E_{qr}C_{rev}}$ mechanism (equation 2, $\mathbf{E}$ as oxidation; $k^0 = 1.0 \cdot 10^{-2}$ cm s^{-1}, $k^f = 10$ s^{-1} and $k^b = 1$ s^{-1}) without (*red*) and with added noise (5% of the peak current) (*black*). Other simulation parameters are specified in Table 1. Currents are normalised to the electrode surface area. Dashed lines (----) indicate the time at which the direction of the d.c. potential ramp is reversed.
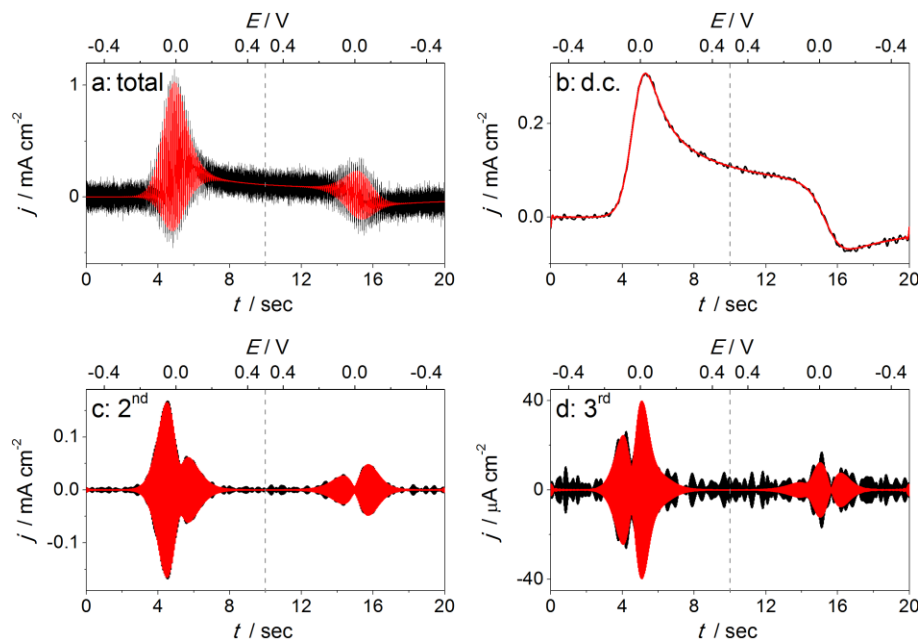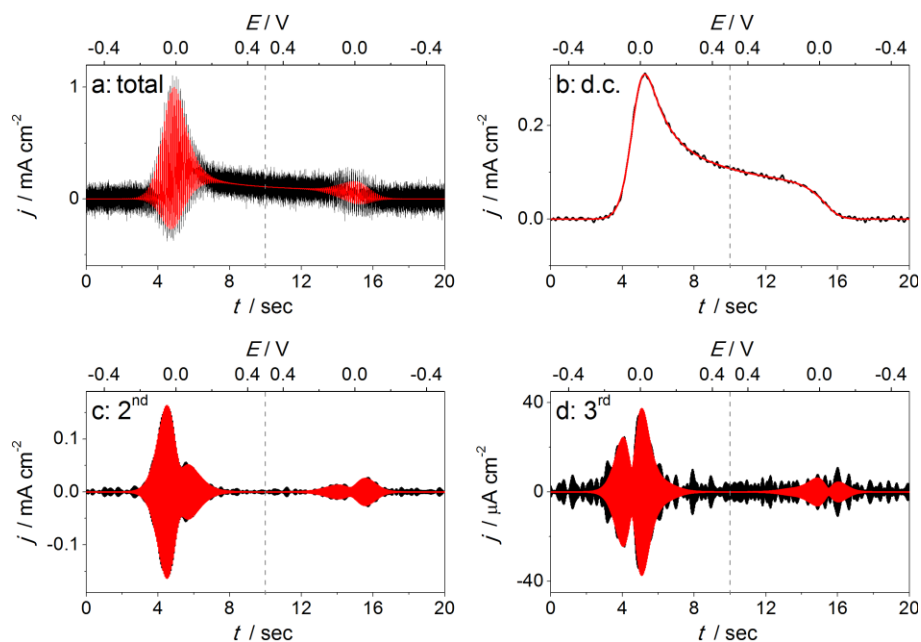
Figure S5. (a) Total current, (b) aperiodic component, (c) 2nd and (d) 5th a.c. harmonic components of an a.c. cyclic voltammogram ($f = 9.00$ Hz; $\Delta E = 0.080$ V; $v = 0.100$ V s^{-1}) simulated for an $\mathbf{E_{qr}C_{irrev}}$ mechanism (equation 2, $\mathbf{E}$ as oxidation; $k^0 = 1.0 \cdot 10^{-2}$ cm s^{-1}, $k^f = 10$ s^{-1}, $k^b = 0$ s^{-1}) without (*red*) and with added noise (5% of the peak current) (*black*). Other simulation parameters are specified in Table 1. Currents are normalised to the electrode surface area. Dashed lines (----) indicate the time at which the direction of the d.c. potential ramp is reversed.

APPENDIX C. BOOTSTRAPPING

Following the preliminary investigation into the ability to estimate parameters from an **EC** reaction mechanism using simulated data with 5% noise and time-domain parameter recovery with the GM algorithm, further insights into the reliability of the reported parameter estimates were sought by using the bootstrapping technique to generate confidence intervals in parameter recovery in transient voltammetry. In this exercise, current-time d.c. or a.c. data and also an equal number of 'noise' measurements, again drawn from a normal distribution with mean zero and standard deviation equal to 5% of the peak current, were generated. Surrogate data sets were then generated by randomly resampling from this recorded noise distribution in an identical way to that described in reference.[S2] The results of five different bootstrapping experiments are presented in Table S1 for two cases: quasi-reversible electron transfer ($k^0 = 10^{-2}$ cm s^{-1}), followed by either a reversible chemical reaction with $k^f = k^b = 100$ s^{-1} (designated here as experiments 1, 4 and 5) or an irreversible chemical reaction with $k^f = 100$ s^{-1} (experiments 2 and 3). Results related to simulated a.c. voltammograms with a frequency of 9 Hz are referred to as experiments 1 and 2, those at 72 Hz as experiments 3 and 4, and d.c. voltammetry is represented as experiment 5 in Table S1. Some of the combinations of parameters employed were chosen to be non-trivial to recover in the presence of 5% noise, based on information provided in Appendix B.

Table S1. Parameters and their standard deviations recovered from 1000 iterations of the bootstrapping algorithm for five different experiments simulated for the **EC** mechanism (equation 2; **E** as oxidation).[a] The values of parameters varied are given in the 'input' rows.[b]

Exp.	Mode	Reading	E^0 / V	k^0 / cm s^{-1}	α	k^f / s^{-1}	k^b / s^{-1}
1	a.c. $f = 9$ Hz	Input	0.000	0.010	0.50	100	100
		Output	0.000 ±0.002	0.010 ±0.001	0.50 ±0.01	101 ±24	101 ±14
2	a.c. $f = 9$ Hz	Input	0.000	0.010	0.50	100	0
		Output	0.000 ±0.004	0.010 ±0.001	0.50 ±0.01	102 ±13	n.a.
3	a.c. $f = 72$ Hz	Input	0.000	0.010	0.50	100	100
		Output	0.000 ±0.001	0.010 ±0.000	0.50 ±0.00	100 ±12	101 ±12
4	a.c. $f = 72$ Hz	Input	0.000	0.010	0.50	100	0
		Output	0.000 ±0.001	0.010 ±0.000	0.50 ±0.00	100 ±4	n.a.
5	d.c.	Input	0.000	0.010	0.50	100	100
		Output	0.000 ±0.002	0.010 ±0.004	0.50 ±0.01	99 ±17	101 ±13

[a] In cases where $k^b = 0$ s^{-1}, an $\mathbf{E_{qr}C_{irrev}}$ model was fitted, otherwise the $\mathbf{E_{qr}C_{rev}}$ one was used.
[b] Other parameters used are: $E_{start} = E_{final} = -0.5$ V, $E_{max} = 0.5$ V, $\Delta E = 0.080$ V for a.c. voltammetry, $v = 0.1$ V s^{-1}, $A = 0.07$ cm^2, $c_A = 1$ mM, $c_B = c_C = 0$ mM, $D_A = D_B = D_C = 2 \cdot 10^{-5}$ cm^2 s^{-1}, $T = 296$ K, $R_u = 0$ Ω, $C_{dl} = 0$ µF cm^{-2}.

Some useful insights are gained from this exercise. In particular, parameter recovery is significantly improved upon introduction of bootstrapping (compare relevant sets of data in Appendices B and C). Nevertheless, in the $\mathbf{E_{qr}C_{rev}}$ cases considered, identification of k^f and k^b values within even a 10% tolerance (one standard deviation) is not achieved, although importantly, the accuracy of the reported parameter estimates, as intimated by their standard

deviations, remains superior when comparing 72 Hz and 9 Hz. a.c. voltammograms. With bootstrapping, even the d.c. technique now also produces reasonable estimates of k^f and k^b, but standard deviations associated with E^0 and k^0 recovery are larger than for the high frequency a.c. experiment. Furthermore, while the reported k^f and k^b values may appear to have been recovered with similar standard deviations from both the a.c. and d.c. voltammetric methods, correlation between these two parameters and the reported value of $K = k^f/k^b$ presented as a scatter plot of pairs of reported k^f and k^b values (Figure S6) clearly confirms that the superiority of the a.c. method is retained.
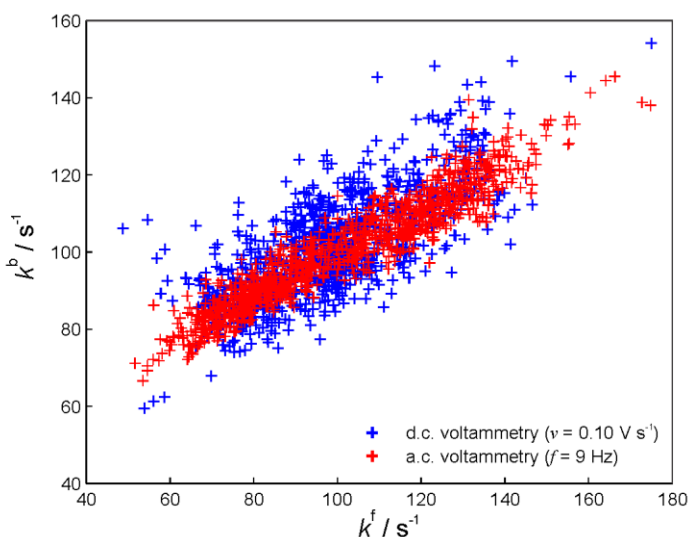

Figure S6. Scatter plot of the values of k^f and k^b recovered from the 1000 iterations of bootstrapping experiments 1 (d.c. voltammetry, blue) and 5 (a.c. voltammetry, red). See Table S1 for parameter details.

This is unambiguosly revealed by noting that the (k^f, k^b) pairs from the a.c. experiment, shown in red, lie closer to a line of best fit which could be drawn through them than the corresponding pairs from the d.c. experiment, shown in blue in Fig. S6. In the a.c. case, calculation of the mean value of $k^f = k^b$, gives an equilibrium constant $K = 1$, which is exactly the value used in the

simulation. The (k^{f}, k^{b}) pairs from the d.c. experiment are not only more scattered, but also correspond to a slightly less accurate equilibrium constant value of $K = 0.97$. In the case of the **E$_{\mathbf{qr}}$C$_{\mathbf{irrev}}$** reaction, the high frequency a.c. method clearly outperforms the lower frequency one, as all parameter estimates have a narrower interval, and indeed at 72 Hz, all parameters are recovered with less than a 5% error.

The detailed impact of the frequency of the a.c. perturbation on the accuracy of recovered parameters, using the example of the quasi-reversible electron transfer followed by an irreversible chemical reaction with $k^{\mathrm{f}} = 100$ s^{-1} as in experiments 2 and 3 of Table S1 are shown in Table S2. Significant gains in the accuracy of all parameters recovered are found as the frequency is increased from 9 Hz to 36 Hz, with only small improvements achieved with further increases in frequency.

Table S2. Summary of results of a bootstrapping exercise undertaken on simulated a.c. voltammograms with 5% added noise for the $\mathbf{E_{qr}C_{rev}}$ mechanism (equation 2; $\mathbf{E}$ as an oxidation process) as a function of frequency. Parameters varied and recovered are E^0, k^0, α and k^f. Values used to produce the simulated voltammograms are listed in the 'Input' row.[a]

	f / Hz	E^0 / V	k^0 / cm s^{-1}	α	k^f / s^{-1}
Input		0.000	0.010	0.50	100
	f / Hz	E^0 / V	k^0 / cm s^{-1}	α	k^f / s^{-1}
	9	0.000 ±0.004	0.010 ±0.001	0.50 ±0.01	102 ±13
	18	0.000 ±0.002	0.010 ±0.001	0.50 ±0.01	101 ±6.4
	27	0.000 ±0.002	0.010 ±0.000	0.50 ±0.01	102 ±4.7
	36	0.000 ±0.002	0.010 ±0.000	0.50 ±0.01	101 ±4.2
Output	45	0.000 ±0.001	0.010 ±0.000	0.50 ±0.01	101 ±4.2
	54	0.000 ±0.001	0.010 ±0.000	0.50 ±0.01	101 ±4.2
	63	0.000 ±0.001	0.010 ±0.000	0.50 ±0.01	101 ±4.2
	72	0.000 ±0.001	0.010 ±0.000	0.50 ±0.01	101 ±4.2
	216	0.000 ±0.001	0.010 ±0.000	0.50 ±0.01	101 ±4.2

[b] Other parameters used are: $E_{start} = E_{final} = -0.5$ V, $E_{max} = 0.5$ V, $\Delta E = 0.080$ V, $v = 0.1$ V s^{-1}, $A = 0.07$ cm^2, $c_A = 1$ mM, $c_B = c_C = 0$ mM, $D_A = D_B = D_C = 2 \cdot 10^{-5}$ cm^2 s^{-1}, $T = 296$ K, $R_u = 0$ Ω, $C_{dl} = 0$ µF cm^{-2}.

APPENDIX D. PROBLEMS ENCOUNTERED IN ATTEMPTS TO USE TRANSIENT AND STEADY STATE D.C. VOLTAMMETRIC METHODS FOR THE QUANTITATIVE ANALYSIS OF THE *trans*-STILBENE$^{-1/-2}$ REDUCTION PROCESS AT MICRO- AND MACRO-DISK ELECTRODES

Commonly, d.c. methods are employed for quantifying **EC** type mechanisms. In this work, transient d.c. cyclic voltammetric experiments as a function of scan rate, along with steady state methods at microelectrodes and rotating disk experiments with macrodisk electrodes as a function of rotation rate have all been examined with respect to quantifying the **EC** *trans*-stilbene$^{-1/-2}$ process. However, none of these traditional or data optimisation approaches were successful for reasons outlined below.

Use of very fast scan rates at macrodisk electrodes required to outrun the **C** step and reach a regime where some level of chemical reversibility is achieved and hence facilitate quantification of an **EC** reaction by the traditional approach (see main text) is problematic in the *trans*-stilbene system due to the very fast kinetics of the chemical step (equation 8; main text), overlap with background charging and solvent reduction currents (background faradaic current that is present in the very negative potential region where the stilbene dianion is generated) as well as the tail of the faradaic current from the first *trans*-stilbene$^{0/1-}$ process and appreciable iR_u drop (R_u is in the range of 50-60 Ω in our macrodisk electrode experiments). Problems, apart from iR_u drop, are evident even under relatively slow scan rate conditions ($v = 1.0$ V s^{-1}) relevant to Fig. D1. Use of a scan rate of 10 V s^{-1} (maximum attempted) was still not sufficient to achieve detectable chemical reversibility in the second reduction step. Use of even higher scan rates needed to achieve this objective are predicted to provide d.c. voltammetric data that are highly distorted by iR_u drop and background current terms according to simulated voltammograms (Fig.D2).
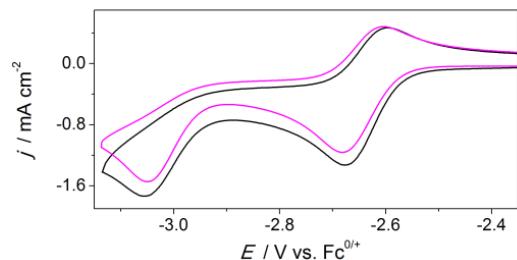
Figure D1. Experimental d.c. cyclic voltammogram obtained at a scan rate of 1.0 V s^{-1} for the reduction of 0.99 mM *trans*-stilbene in CH$_3$CN (0.10 M Bu$_4$NPF$_6$) at a GC electrode (*black*) and data simulated using parameters specified in Table 4 of the main text that are relevant to d.c. cyclic voltammetry (*magenta*). See references[S12,13] for further experimental details.
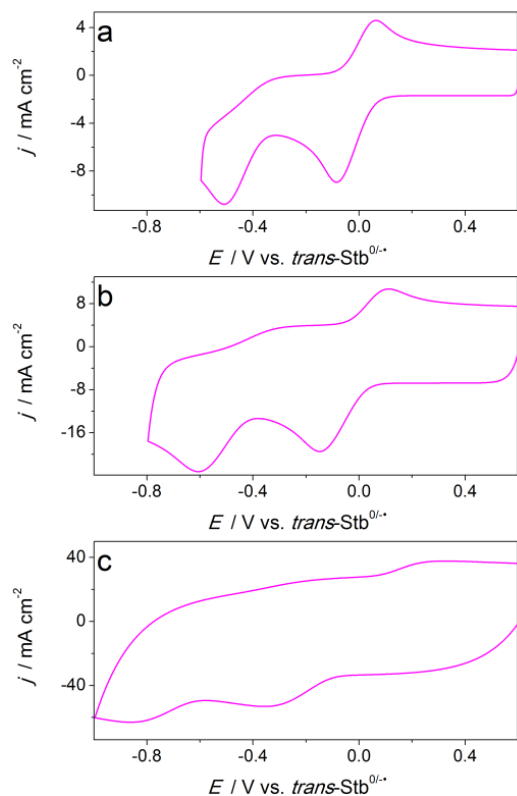

Figure D2. D.c. voltammograms simulated for the reduction of 0.99 mM *trans*-stilbene in CH$_3$CN (0.10 M Bu$_4$NPF$_6$) with R_u = 60 Ω, v = 50 (a), 200 (b) and 1000 V s^{-1} (c) and other parameters specified in Table 4 of the main text that are relevant to d.c. cyclic voltammetry.

Despite the fact that conventional or multi-parameter data optimisation methods failed to achieve quantification of the *trans*-stilbene **EC** process using d.c. voltammetric data, it is of course possible to use parameters successfully deduced from a.c. voltammetry and simulate d.c. responses predicted on this basis. As expected, and as shown in Fig D1, 'good' agreement is achieved with experimental data and d.c. cyclic voltammograms simulated using electrode kinetic parameters deduced from data optimisation of a.c. voltammetry.

Quantitative analysis of the near steady-state voltammetric data obtained for the second reduction step of *trans*-stilbene in CH_3CN at microelectrodes also is hampered by significant overlap from background faradaic current that is present in the very negative potential region where the stilbene dianion is generated. This is exemplified in Fig. D3 by the sloping baseline prior to the onset of the stilbene$^{-\bullet/-2}$ and even more sloping limiting current obtained at an 11 μm carbon fibre microdisk electrode. The background current at a 10 μm platinum microdisk is even more severe. In principle, the background processes can be studied in separate experiments and modelled to be included in simulation of the data obtained for reduction of *trans*-stilbene. However, this would introduce additional and significant uncertainty to analysis due to far from perfect reproducibility of the background current and very high sensitivity of the electron transfer kinetics for *trans*-stilbene reduction on the state of the electrode surface. Excursions of the potentials to very negative values results in poisoning of the electrode, especially carbon based ones, and degradation of the kinetics of the stilbene reduction. Therefore, each voltammogram should be obtained with a freshly polished electrodes (as was done in our experiments), and using the same electrode to study background processes and *trans*-stilbene reduction is not feasible. Thus, use of a series of carbon based microelectrodes of variable radii to quantify this **EC** process is not practical.
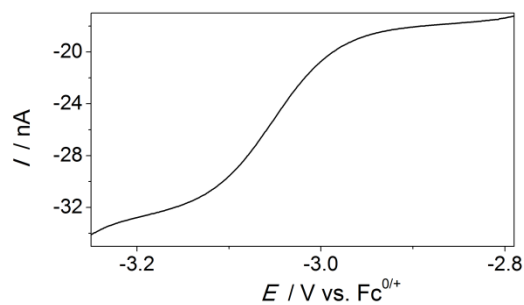
Figure D3. Near steady state voltammogram ($v = 0.005$ V s^{-1}) obtained for the *trans*-stilbene$^{-\bullet/2-}$ process derived from reduction of *ca* 3.3 mM stilbene in CH$_3$CN (0.10 M Bu$_4$NPF$_6$) at a carbon fibre microdisk electrode (diameter 11 μm). See references[S12,13] for further experimental details.

Finally, it is noted that the steady state response at a rotating disk electrode suffers even more severely from overlap with the background current, particularly at high electrode rotation speeds needed to quantify the **EC** process (see Figure S1 of reference[S13]).
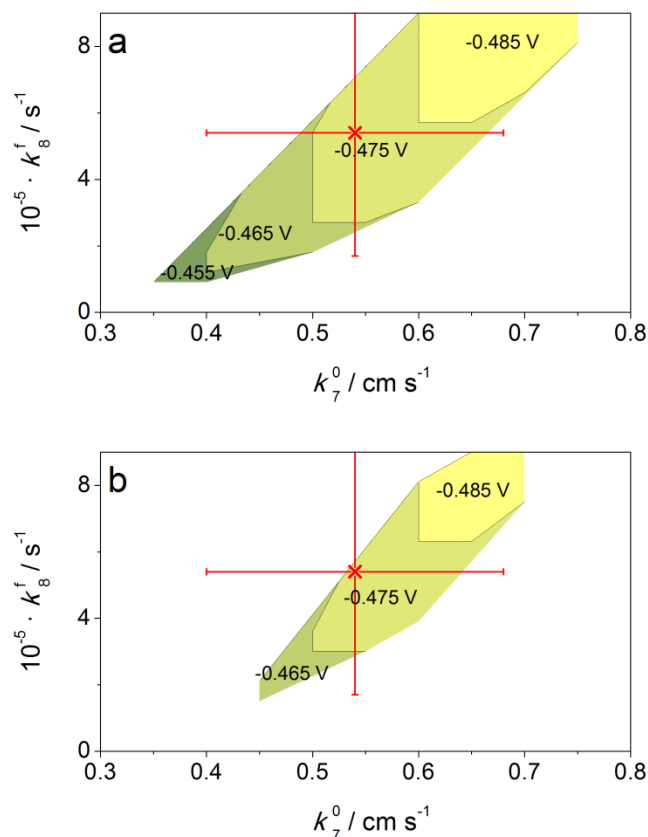
Figure S7. Correlation between the 'optimal' values of k^0_7 and k^f_8 providing the lowest objective, $\Psi_{Nim} < 0.15$ (a) or 0.14 (b) when fitting a simulation based on reactions 6-8 to the 1st to 8th harmonic components of an experimental a.c. cyclic voltammogram for the second process in the reduction of 0.99 mM *trans*-stilbene in CH_3CN (0.10 M Bu_4NPF_6) using Nimrod/G parameter sweep analysis on Ψ_{Nim} as a function of E^0_7, k^0_7 and k^f_8. Values and coloured sections show the corresponding 'optimal' E^0_7 values. k^0_7 and k^f_8 values outside the coloured regions correspond to $\Psi > 0.15$ (a) or 0.14 (b). Other experimental and simulation parameters are as in Table 4. × and associated confidence intervals show the [k^0_7, k^f_8] combination and standard deviations derived from the Nimrod/O optimisation studies reported in Table 4).

SUPPORTING REFERENCES

(S1) Morris, G. P.; Simonov, A. N.; Mashkina, E. A.; Bordas, R.; Gillow, K.; Baker, R. E.; Gavaghan, D. J.; Bond, A. M. *Analytical Chemistry* **2013**, *85*, 11780-11787.

(S2) Simonov, A. N.; Morris, G. P.; Mashkina, E. A.; Bethwaite, B.; Gillow, K.; Baker, R. E.; Gavaghan, D. J.; Bond, A. M. *Analytical Chemistry* **2014**, *86*, 8408-8417.

(S3) http://www.garethkennedy.net/MECSim.html. Accessed on 25.03.2016.

(S4) Lee, C.-Y.; Bullock, J. P.; Kennedy, G. F.; Bond, A. M. *The Journal of Physical Chemistry A* **2010**, *114*, 10122-10134.

(S5) Rudolph, M.; Reddy, D. P.; Feldberg, S. W. *Analytical Chemistry* **1994**, *66*, 589A-600A.

(S6) Gavaghan, D. J.; Bond, A. M. *Journal of Electroanalytical Chemistry* **2000**, *480*, 133−149.

(S7) Mocak, J.; Feldberg, S. W. *Journal of Electroanalytical Chemistry* **1994**, *378*, 31-37.

(S8) Sulli, E.; Mayers, D. *An introduction to Numerical Analysis*; Cambridge University Press, 2003.

(S9) Brent, R. P. *Algorithms for Minimization without Derivatives*; Prentice Hall, 1973.

(S10) Savéant, J. M.; Vianello, E. *Electrochimica Acta* **1963**, *8*, 905-923.

(S11) Ruzić, I.; Feldberg, S. *Journal of Electroanalytical Chemistry and Interfacial Electrochemistry* **1974**, *50*, 153-162.

(S12) Abdul-Rahim, O.; Simonov, A. N.; Boas, J. F.; Rüther, T.; Collins, D. J.; Perlmutter, P.; Bond, A. M. *The Journal of Physical Chemistry B* **2014**, *118*, 3183-3191.

(S13) Abdul-Rahim, O.; Simonov, A. N.; Rüther, T.; Boas, J. F.; Torriero, A. A. J.; Collins, D. J.; Perlmutter, P.; Bond, A. M. *Analytical Chemistry* **2013**, *85*, 6113-6120.